Dielectric resonator to measure surface resistance of accelerator components at room temperature and 77 K

Kristóf Brunner,* Patrick Krkotić,† Pedro Costa Pinto, Eduardo Gibbons Diaz-Rato, Stephan Pfeiffer, Wilhelmus Vollenberg, and Sergio Calatroni
CERN, Esplanade des Particules 1, 1217 Meyrin, Switzerland

Dániel Barna
Wigner RCP, Konkoly-Thege Miklós út 29-33, 1121 Budapest, Hungary

Montse Pont
ALBA Synchrotron Light Source, Carrer de la Llum 2-26, 08290 Cerdanyola del Valles, Barcelona, Spain

Joan O'Callaghan
Commsenslab, Department of Signal Theory and Communications, Universitat Politècnica de Catalunya (UPC), C/Jordi Girona 1, 08034 Barcelona, Spain

(Received 9 March 2023; accepted 26 June 2023; published 17 August 2023)

We measured the surface resistance of titanium, amorphous carbon, and nonevaporable getter (NEG) coatings on copper samples, representative of surface treatments of beam-facing components in the High-Luminosity Large Hadron Collider at CERN. Measurements were done at room temperature as well as at liquid nitrogen temperature (77 K) by means of a novel large dielectric resonator operating at 3.4 GHz. The impact of a 100 to 400 nm titanium layer or a 50-nm amorphous carbon layer was negligible both at room temperature and down to 77 K in comparison to copper, while a thick (1140 nm) NEG layer showed a measurable increase in the surface resistance, being more significant at low temperature. The dielectric resonator proved to be a useful tool to characterize the surface resistance of flat samples with different surface treatments and sizes up to 10 cm for accelerator applications. Furthermore, its construction and operation are much simpler compared to other test devices currently in use, and it can provide accurate experimental data for the evaluation of the beam coupling impedance.

DOI: 10.1103/PhysRevAccelBeams.26.083101

I. INTRODUCTION

In this study, we discuss the surface resistance measurement method of using a large ($d = 105$ mm, $h = 20$ mm) rf dielectric resonator (from now DR) of Hakki-Coleman type [1] as well as presenting the first measurement results on several samples. The motivation for the research was to prove the usefulness of such a large DR in the measurement of the surface resistance of materials, coatings, and surface treatments for accelerator components in the frequency range between 1 and 4 GHz. Measuring the surface resistance of a given coated sample allows for the estimation of the heating effect of the image currents running on the surfaces exposed to the beam and is also related to the beam coupling impedance ([2,3]). Even though a multiple-frequency measurement would provide even more information, at this stage, we only aimed at using a single mode of the cavity to demonstrate the principle, resulting in a single-frequency measurement. The samples tested are disk shaped, forming the top of a cylindrical cavity, while the lateral wall and the bottom of the cavity are made out of copper (as seen in Figs. 1 and 2). The first advantage of dielectric loading is that it lowers the measured resonant frequency to 3.41 GHz so that it is closer to the region of interest, which for LHC and HL-LHC beam screen components is between 0 and 3 GHz [2]. In the past, similarly sized measurement devices were tested, for example, the three-choked pillbox cavity ([4]) can also measure flat samples with diameters of 100 mm, but its frequency (7.8 GHz) is twice as high as the frequency of the DR. Other groups have successfully used small tapered cavities using the TE011 mode (same as what we use in the DR) but without a dielectric loading ([5,6]),

*kristof.brunner@cern.ch
Also at Wigner RCP, ELTE University, Budapest.
†patrick.krkotic@cern.ch

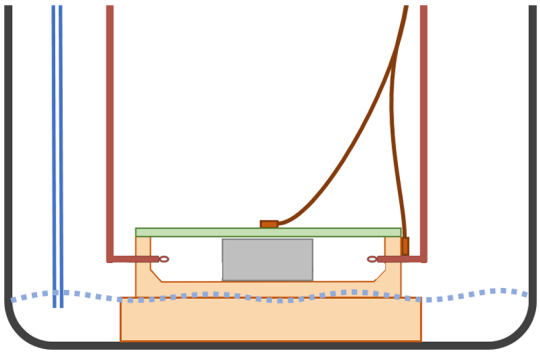

FIG. 1. Schematic of the measurement setup. The base, the bottom, and the side walls of the cavity (all copper) are orange. The sample measured is green, with a temperature sensor on the top and side. The single crystal sapphire dielectric is gray. The dashed line shows the level of the liquid nitrogen during the cooldown. The whole setup is sitting on the bottom of a 100 L cryostat.

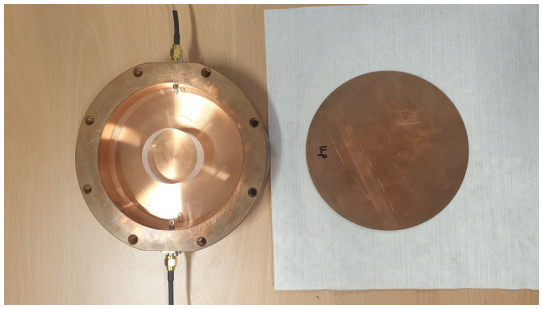

FIG. 2. Image of the open DR. The top plate is fixed via eight screws on the circumference of the cavity.

their resonant frequencies thus are significantly higher than ours, but the method used is very similar. In upcoming measurements with the use of other dielectric materials such as TiO_2 (rutile) or $TiSrO_3$, the frequency of the DR could be reduced even further. The second advantage of dielectric loading is that it concentrates the electric field and thus the currents running in the cavity walls to the center of the sample disk. This way if the edge of the sample is not coated homogeneously, it does not influence the outcome of the measurement.

The samples tested were copper plates covered by different thin film coatings, commonly used as the surface coating of accelerator components. First, we measured a simple copper plate to have a baseline measurement to compare our results. Then we tested amorphous carbon-coated copper plates. Amorphous carbon (a-C) coating with an underlayer of titanium is planned to be used in the High-Luminosity LHC (HL-LHC) in order to reduce the secondary electron yield of the beam screen surface, thus mitigating the electron cloud effect [7–9]. Finally, we tested four plates coated with TiZrV nonevaporable getter (NEG) such as used at CERN [10].

Further samples planned for being tested are for example ones that have undergone laser surface structuring in order to reduce their secondary electron yield [11,12]. Other accelerator components made out of different materials can be tested as well with some simple modifications to our setup. One such example is a special collimator of HL-LHC that has molybdenum coating on molybdenum graphite jaws to reduce the impact of the impedance on beam stability [13].

II. MEASUREMENT TECHNIQUE

The base of the cavity was machined out of a single block of copper. The inside diameter is 105 mm, with a height of 20 mm. The measured sample closes this cavity as the top plate (as seen in Fig. 1). In the center of the cavity, we place a single crystal sapphire ($\alpha - Al_2O_3$) with a crystal orientation (0001), a diameter of 40 mm and a height of 19.5 mm, 0.5 mm lower than the internal height of the cavity to ensure that we do not touch and scratch the surface of the sample. It had to be verified using CST simulations that this gap does not change the field patterns significantly [14]. The crystal orientation was chosen to ensure that the electric field is perpendicular to the c axis (the axis perpendicular to the hexagonal base of the sapphire crystal structure) in any TE mode. This way, the dielectric can be modeled as having a homogeneous dielectric constant (note that this is not true for TM modes).

A candidate mode for the measurement is the TM010 mode with a frequency of 1.5 GHz. In this mode, the surface currents run from the center of the circular disk outwards radially and across the contact point between the top plate and the cavity wall. Therefore, losses in this mode are extremely sensitive to the contact resistance and the force pushing the sample plate onto the cavity. Because of this, the measurement using this mode was not well reproducible at room temperature so we discarded the use of TM010 altogether for this test.

More reproducible measurements are obtained with the TE011 mode, seen in Fig. 3. The frequency of this mode with our cavity dimensions is 3.41 GHz, which is still representative of the high-frequency part of the HL-LHC beam spectrum [2]. In this mode, surface currents run in a circular path (seen in Fig. 4), so they do not traverse from the sample plate to the sidewall of the cavity. This means that contact resistance does not play any role in the quality factor measurement. The electric field and the surface currents in the TE011 mode can be seen in Figs. 3 and 4, respectively.

At room temperature, the measured frequency of the mode of interest corresponds to a simulation with a dielectric factor of 9.39 which is in agreement with the literature value $\epsilon_\perp = 9.33$.

The schematic of the measurement setup at the bottom of a cryostat can be seen in Fig. 1. The cooling is done using liquid nitrogen. A large supporting piece of copper is

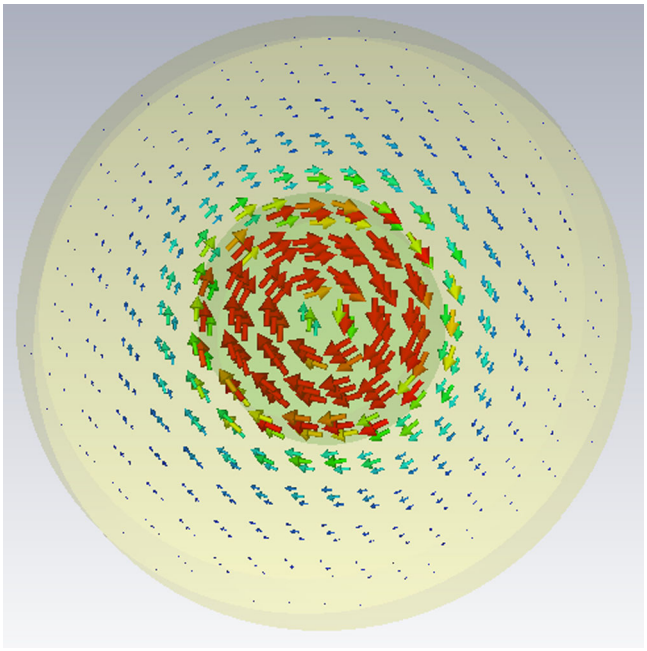

FIG. 3. Electric field in the TE011 mode.

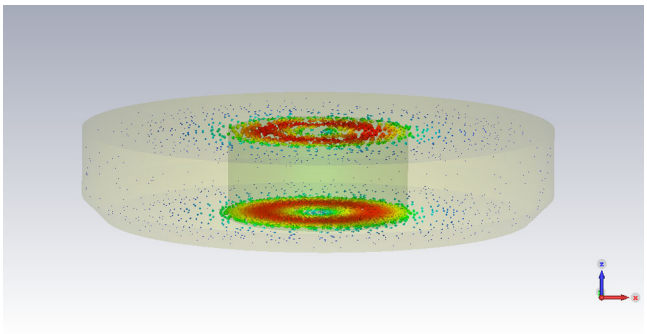

FIG. 4. Surface currents in the TE011 mode.

cooled directly by the liquid which indirectly cools the cavity via heat conduction. This is done to avoid liquid getting into the cavity and potentially moving the sapphire from the center. To measure the temperature dependence of the quality factor, we collected data points continuously while letting the setup slowly warm up during the night. The Python Automatized Night-time Data Acquisition (PANDA) tool was developed to monitor the measurement.

The different S-parameters of the cavity were measured by a Rhode and Schwarz ZNB 4, while the temperature measurement was done using two different PT100 sensors connected to a current source and voltage readout according to a simple four-cable measurement method. One of the temperature sensors was installed in the center of the 2-mm thick sample plate, the other one on the side wall of the cavity (both outside the cavity), as seen in Fig. 1. Both of them had cryogenic grease (Apiezon N) under them to ensure good thermal contact and Kapton tape was used to

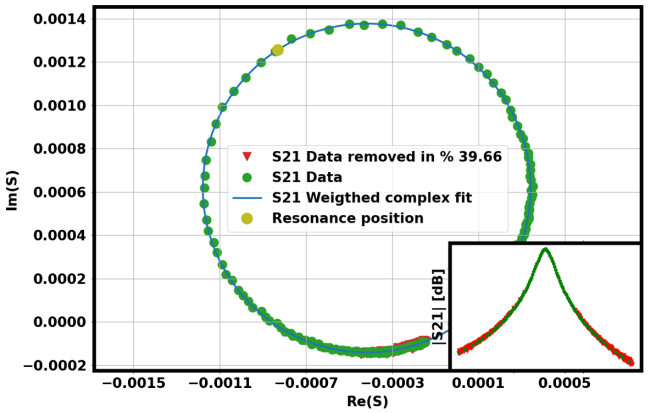

FIG. 5. The raw data fit with a circle in the complex plane by ARPE. For more information on the process of data analysis of ARPE, see [15].

hold them down during cooldown. Since the cavity and sample plate are both constructed out of copper, which has very high heat conductivity, the two measured temperatures were never further than 1 to 2 K from each other, so the temperature of the entire DR can be considered to be uniform.

The touchstone (S2P) files of the measurements were saved containing the magnitude and phase of S11, S12, S21, and S22, then postprocessing of the signals was done using the tool called algorithm for resonator parameter extraction (ARPE) [15].

In a symmetrical transmission response, the loaded quality factor would be calculated as $Q_L = f_0/\Delta f$, where f_0 is the resonant frequency of the mode, and Δf is the full-width at half maximum. Due to parasitic effects, this simple method would not give an accurate unloaded quality factor. What ARPE does instead is first find the resonant peak in the transmission response data and fit the data with a partial circle in the complex plane. The raw S21 data of measurement being filtered and fit via ARPE can be seen in Fig. 5. This way it is able to remove contributions such as cross-talk between the resonator ports (leading to the asymmetry of the peak). From this least-squares circle fit, the algorithm determines the loaded quality factor and resonance frequency of the mode. This method is much more resilient against any disturbances or noise in the signal. To get the unloaded quality factor from the loaded one, ARPE uses the equation $Q_0 = (1 + \beta_1 + \beta_2)Q_L$ where β_1 and β_2 are the coupling factors. Two circles are fit to the reflection responses (S11, S22) in the complex plane using the least-squares method. From the fitting parameters, ARPE calculates the coupling factors.

In our DR, the electrical losses can be separated into four contributions, the resistive losses in the top, bottom, and side walls, respectively, and the dielectric losses in the sapphire. The unloaded quality factor of the resonator can then be written as [16]:

$$\frac{1}{Q_0} = \frac{1}{Q_{\text{top}}} + \frac{1}{Q_{\text{bot}}} + \frac{1}{Q_{\text{side}}} + p\ \tan(\delta), \tag{1}$$

$$\frac{1}{Q_0} = \frac{R_{S,\text{top}}}{\Gamma_{\text{top}}} + \frac{R_{S,\text{Cu}}}{\Gamma_{\text{bot}}} + \frac{R_{S,\text{Cu}}}{\Gamma_{\text{side}}} + p\ \tan(\delta), \tag{2}$$

where $R_{S,\text{top}}$ and $R_{S,\text{Cu}}$ are the surface resistance of the top plate and the surface resistance of copper, $\Gamma_{\text{top,bot,side}}$ are the corresponding geometry factors. The quantity p represents the filling factor regarding the dielectric. All geometry factors and the filling factor were determined using an eigenmode simulation of the setup built in CST Studio Suite. The uncertainty of these values contributes to the overall uncertainty of our errors, but we estimate them to influence the results by less than 1%, while measurement uncertainties contribute significantly more (for example, upon disassembling and reassembling the setup we see up to 2% change in the measured surface resistance). The dielectric loss tangent of sapphire [$\tan(\delta)$] is orientation and temperature dependent and was taken from the literature [17]. At 77 K, the dielectric losses are vanishingly small. From Eq. (2), we can express the surface resistance of the top plate as

$$R_{s,\text{top}} = \Gamma_{\text{top}}\left(\frac{1}{Q_0} - p\ \tan(\delta) - \frac{R_{s,\text{Cu}}}{\Gamma_{\text{bot}}} - \frac{R_{s,\text{Cu}}}{\Gamma_{\text{side}}}\right). \tag{3}$$

III. SAMPLE PREPARATION

We tested 11 sample plates altogether, all plates are created using 2-mm thick Cu-OFE (UNS C10100) round plates, with a diameter of 110 mm. Disk number 0 is a simple copper plate used as a baseline for the other measurements. The other ten samples have single or multilayer coatings. The plates were cleaned and passivated with chromic acid prior to coating.

All Ti and a-C coatings were performed using a planar magnetron sputtering source after 8 h of bake-out at 120°C in a vacuum system. The pressure before coating was $P_{\text{limit}} = 1 \times 10^{-7}$ mbar. The titanium and the graphite target were placed 145 mm away from the sample. Argon was used as the discharge gas. During the application of the first titanium layer, the pressure was 2.4×10^{-3} mbar (signaled as Ti (1) in Table I), for every other Ti and a-C layer the argon pressure was 9.7×10^{-3} mbar.

The NEG coatings were prepared using similar pump-down and bake-out parameters. Instead of argon, krypton was used as the discharge gas, at approximately 1×10^{-3} mbar pressure. Two different methods were used: high-power impulse magnetron sputtering (HiPIMS) and direct current magnetron sputtering (DCMS). Using both methods, two samples were coated with different layer thicknesses, as seen in Table I.

TABLE I. Thickness of different layers of the ten coated samples.

	Ti (1) (nm)	Ti (2) (nm)	a-C (nm)	NEG (HiPIMS) (nm)	NEG (DCMS) (nm)
1	70				
2	70	70			
3	70	70	50		
4	140				
5	140	210			
6	140	210	50		
7				1140	
8					1170
9				240	
10					250

Together with each round plate, two witness samples were coated: one made out of glass and the other out of copper. The glass sample was used for dc resistivity measurement and the copper one for the measurement of the layer thicknesses. The dc sheet resistances of the different NEG layers were measured separately by a 4-point probe on the coated glass witness sample. Disks 7–10 had measured dc sheet resistances of $(1.77 \pm 0.12)\ \Omega$, $(1.74 \pm 0.04)\ \Omega$, $(12.79 \pm 0.52)\ \Omega$, and $(13.24 \pm 0.84)\ \Omega$, respectively. From this, knowing the thickness of the layers, we calculated the resistivity of the different coatings. Then the theoretical surface resistances of the copper plus NEG multilayer sheets were calculated using the technique described in [18]. In the case of the Ti and a-C coatings, this value is not different from the surface resistance of copper since the thicknesses of the coatings are significantly lower than the skin depth at the frequency of the measurement ($\delta_{\text{Ti}} = 5.2\ \mu\text{m}$, $\delta_{\text{a-C}} = 43.2\ \mu\text{m}$). In the case of the NEG coatings, the calculated surface resistance values are included in Table II.

TABLE II. Measured unloaded quality factors and the resulting surface resistances, compared with theoretical values from electrical resistivity.

	Q_0	R_s (mΩ)	$R_{s,\text{theory}}$ (mΩ)
0	13606 ± 217	15.35 ± 0.21	15.10 ± 0.08
1	13480 ± 272	15.50 ± 0.26	
2	13525 ± 301	15.44 ± 0.29	
3	13476 ± 262	15.50 ± 0.25	
4	13522 ± 326	15.44 ± 0.31	
5	13504 ± 261	15.47 ± 0.25	
6	13446 ± 298	15.54 ± 0.28	
7	13131 ± 256	15.94 ± 0.24	15.80 ± 0.10
8	13179 ± 306	15.88 ± 0.29	15.80 ± 0.10
9	13380 ± 281	15.62 ± 0.27	15.10 ± 0.08
10	13445 ± 281	15.54 ± 0.27	15.10 ± 0.08

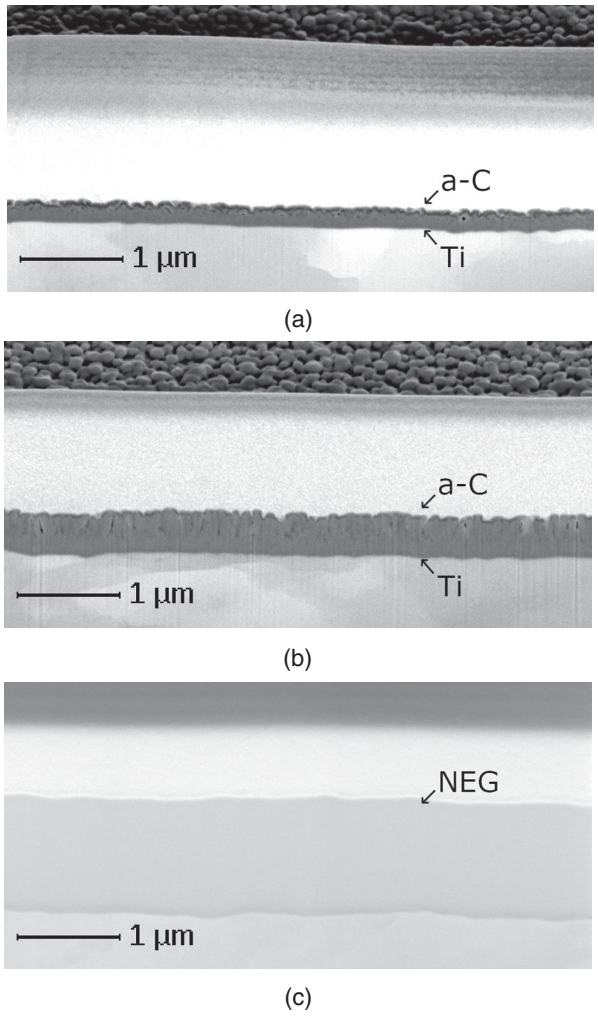

FIG. 6. SEM cross-sectional images of samples 3 (a), 6 (b), and 7 (c).

A Zeiss Crossbeam 540 Focused Ion Beam (FIB)/scanning electron microscope (SEM) system with field emission gun (FEG) was used to perform cross-sectional milling. A platinum protection layer was deposited on the samples before milling in order to preserve the surface layers. The in-lens secondary electron detector was used for imaging the cross sections as it provided the best electron contrast and the layer thicknesses were then measured by SEM imaging. The resulting cross-sectional images can be seen in Fig. 6.

IV. RESULTS AT ROOM TEMPERATURE

The results of the room temperature measurements can be seen in Fig. 7 and Table II. The uncertainties of these results come from the error of the quality factor measurement, the geometrical uncertainties, the uncertainty of the dielectric losses in the sapphire, as well as the variation of the quality factor if we disassemble and reassemble the resonator with the same top plate. The measurement of the

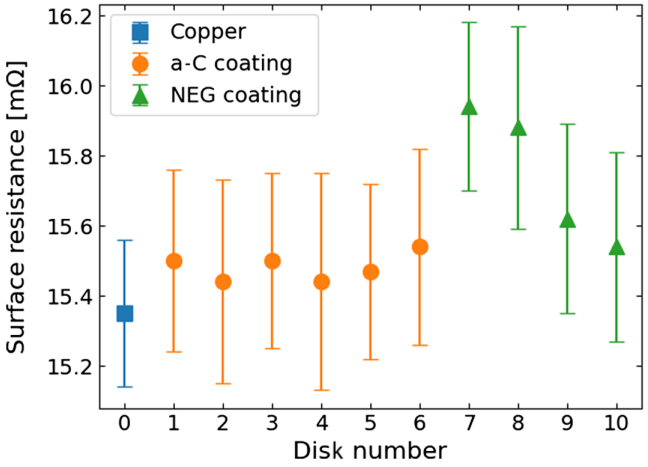

FIG. 7. Results of the room temperature measurements, each disk was measured 5 times.

plain copper plate should result in the theoretical surface resistance of copper, with any deviation from it being caused by the systematic error of our measurement, we can use this to estimate the systematic error, which should also be applicable to the measurement of the other samples.

As expected from our calculations discussed in the previous section, we did not see a significant change in the surface resistance of the first six samples but measured around a 5% increase in the surface resistance of the samples coated by a thick layer of NEG.

V. RESULTS AT 77 K AND DISCUSSION

A full temperature sweep from 77 to 300 K was done on every sample. During the sweep, a temperature gradient of up to 2 K was measured between the center of the top plate and the side wall of the DR. This, however, only influenced the results to a small extent and was impossible to avoid during warmup or cooldown of the setup unless using a more complicated cooling method. The cooldown usually took around 2 h, while the warmup was done overnight. Often some noise was visible in the signal close to room temperature. After some investigation, it turned out that this is caused by water condensation on the top of the cryostat, which first freezes, but as the temperature reaches 0 °C the ice melts and water starts dripping onto the temperature sensor. Due to this, we had to separate the cryogenic ($<$250 K) and the room temperature measurements in our results and discussion.

From 77 to 250 K, the resonant frequency changes approximately 20 MHz. This was mainly caused by the change in the dielectric factor of sapphire (see [17]). The resonant frequency measured for a few samples as a function of temperature is visible in Fig. 8.

In Fig. 9, one can see the relative change in the temperature dependence of the surface resistance of the different samples normalized with the surface resistance

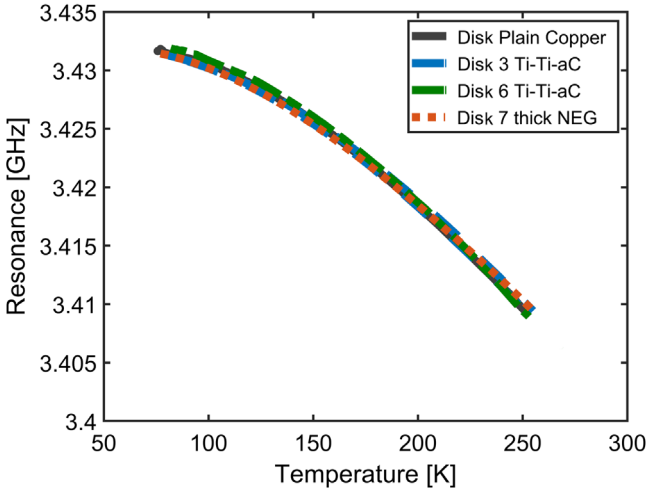

FIG. 8. Resonant frequency as a function of temperature for four disks.

of disk 0 at the corresponding temperature. Figures 9(a) and 9(b) show that the surface resistance of Ti and a-C coated samples does not deviate from the surface resistance of copper by more than 5% over the entire temperature range (disks 1–6). Though in the room temperature measurement, we consider 5% to be a significant change (since the standard deviation measured at room temperature was only 3%), in this one, the temperature measurement's uncertainty influences the measured resistance ratio significantly. This is the reason for the significantly higher (3%–7%) error bars on our results. Thus we consider, that in line with our theoretical expectations, the measured surface resistance of disks 1–6 is not significantly different from plain copper. As discussed earlier, the layer thickness is much smaller than the penetration depth. These results corroborate those of [19] which were measured on similar coatings at the fixed temperature of 4.2 K only and at a lower frequency range. In our case, the higher frequency allows exploring a shallower depth, still confirming the "transparency" of these coatings. It should be mentioned that the present experimental technique is of much simpler implementation compared to that of [19] and allows exploring a significant temperature range relevant to the HL-LHC accelerator operations.

Finally, Fig. 9(c) shows the results of the four NEG-coated samples. Although NEG is not commonly used in cryogenic environments, it is nevertheless useful to assess its surface resistance. The thin NEG coating does not influence the surface resistance within experimental uncertainty, while the thick NEG coating increases it by more than 5%–15%. This is to be expected as the penetration depth for our coating is around 9.3 μm at room temperature and the coatings are more than 1.2 μm thick. Similar results were obtained in [4], even though in that case measurements were performed at a higher frequency and at room

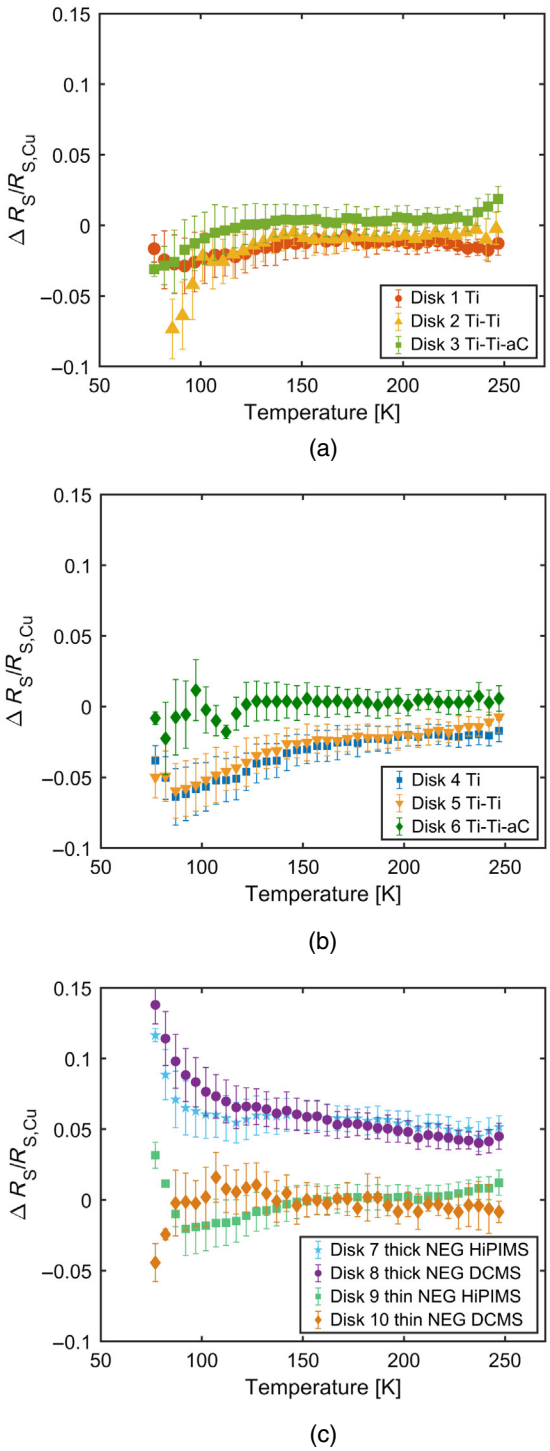

FIG. 9. Relative surface resistance with respect to the copper plate (disk 0) as a function of the temperature. Disk 1–3 in (a), 4–6 in (b), and 7–10 in (c).

temperature. From our measurements, the fact that the results as a function of temperature show a negative slope indicates a smaller temperature dependence of the surface resistance of NEG coating compared to that of copper, although a proper quantitative evaluation is not feasible due to experimental uncertainties.

VI. CONCLUSION

A large dielectric resonator has been designed and fabricated to measure the surface resistance of large coated or surface-treated samples at the few-GHz range, in order to help assess their impact in accelerator applications, such as the HL-LHC at CERN. The measured results on a-C and NEG-coated samples allow inferring a negligible effect on HL-LHC beam operations of any beam-facing components having these coatings in their corresponding environment (NEG only above 190 K) [20]. Nevertheless, the LHC beam frequency spectrum lies below our test frequency of 3.41 GHz. In order to reach lower frequencies, one could design a dielectric resonator of even larger dimensions, but the production of a large sapphire single-crystal can significantly raise the cost, as well as being impractical for sample production. Using a different dielectric material with an even higher dielectric constant such as single-crystal TiO_2 (rutile) or $TiSrO_3$ would then be a better option, and the procurement of these materials in the required size is being investigated.

We are planning in the future to measure samples that have undergone laser surface structuring in order to reduce their secondary electron yield. The current paths on the top plate in the TE011 mode are concentric, we will thus be able to differentiate between treatments with radial versus concentric grooves. This setup will provide analysis similar to [19] with different laser parameters. A possible extension of our DR system to operate at lower temperatures in a liquid helium cryostat is also envisaged while still keeping a comparatively simple sample geometry and easy operating procedures.

ACKNOWLEDGMENTS

The authors acknowledge the stimulating discussions with F. Caspers, as well as the work conducted by several people on the preparation and metrological measurement of the samples, namely S. Fiotakis, C. Serafim, and A. Moros.

[1] B. Hakki and P. Coleman, A dielectric resonator method of measuring inductive capacities in the millimeter range, IRE Trans. Microwave Theory Tech. **8**, 402 (1960).

[2] E. Métral, Rf heating from wake losses in diagnostics structures, in *Proceedings of IBIC2013, Oxford, UK* (2013), p. 929, http://accelconf.web.cern.ch/IBIC2013/papers/thbl1.pdf.

[3] S. Calatroni, E. Bellingeri, C. Ferdeghini, M. Putti, R. Vaglio, T. Baumgartner, and M. Eisterer, Thallium-based high-temperature superconductors for beam impedance mitigation in the future circular collider, Supercond. Sci. Technol. **30**, 075002 (2017).

[4] O. B. Malyshev, L. Gurran, P. Goudket, K. Marinov, S. Wilde, R. Valizadeh, and G. Burt, RF surface resistance study of non-evaporable getter coatings, Nucl. Instrum. Methods Phys. Res., Sect. A **844**, 99 (2017).

[5] C. Accettura, D. Amorim, S. Antipov, A. Baris, A. Bertarelli, N. Biancacci, S. Calatroni, F. Carra, F. Caspers, E. Garcia-Tabares Valdivieso, J. Guardia Valenzuela, A. Kurtulus, A. Mereghetti, E. Metral, S. Redaelli, B. Salvant, M. Taborelli, W. Vollenberg, and W. Vollenberg, Resistivity characterization of molybdenum-coated graphite-based substrates for High-Luminosity LHC Collimators, Coatings **10**, 361 (2020).

[6] S. Yue, S. Tian, N. Wang, T. Xin, J. Wang, and G. Xu, Measurements on the conductivity of copper coating with resonant cavity, Radiat. Detect. Technol. Methods **7**, 248 (2023).

[7] F. Zimmermann, Review of single bunch instabilities driven by an electron cloud, Phys. Rev. ST Accel. Beams **7**, 124801 (2004).

[8] M. Tobiyama, J. W. Flanagan, H. Fukuma, S. Kurokawa, K. Ohmi, and S. S. Win, Coupled bunch instability caused by an electron cloud, Phys. Rev. ST Accel. Beams **9**, 012801 (2006).

[9] O. Aberle, I. Béjar Alonso, O. Brüning, P. Fessia, L. Rossi, L. Tavian, M. Zerlauth, C. Adorisio, A. Adraktas, M. Ady, J. Albertone, L. Alberty, M. Alcaide Leon, A. Alekou, D. Alesini, B. A. Ferreira, P. A. Lopez, G. Ambrosio, P. Andreu Munoz, and M. Anerella, High-Luminosity Large Hadron Collider (HL-LHC): Technical design report, CERN, Geneva, CERN Yellow Reports: Monographs, 2020, Vol. **10**.

[10] P. Chiggiato and P. Costa Pinto, Ti–Zr–V non-evaporable getter films: From development to large scale production for the Large Hadron Collider, Thin Solid Films **515**, 382 (2006).

[11] M. Pivi, F. K. King, R. E. Kirby, T. O. Raubenheimer, G. Stupakov, and F. Le Pimpec, Sharp reduction of the secondary electron emission yield from grooved surfaces, J. Appl. Phys. **104**, 104904 (2008).

[12] S. Calatroni, E. Garcia-Tabares Valdivieso, H. Neupert, V. Nistor, A. T. Perez Fontenla, M. Taborelli, P. Chiggiato, O. Malyshev, R. Valizadeh, S. Wackerow, S. A. Zolotovskaya, W. A. Gillespie, and A. Abdolvand, First accelerator test of vacuum components with laser-engineered surfaces for electron-cloud mitigation, Phys. Rev. Accel. Beams **20**, 113201 (2017).

[13] S. A. Antipov, C. Accettura, D. Amorim, A. Bertarelli, N. Biancacci, R. Bruce, E. Carideo, F. Carra, J. Guardia Valenzuela, A. Mereghetti, E. Métral, S. Redaelli, B. Salvant, and D. Valuch, Transverse beam stability with low-impedance collimators in the high-luminosity large hadron collider: Status and challenges, Phys. Rev. Accel. Beams **23**, 034403 (2020).

[14] C. Sans, M. O'Callegham, D. Sancho, R. Pous, J. Fontcuberta, J.-F. Liang, and G.-C. Liang, Full-wave analysis of the image hybrid dielectric/HTS resonator, IEEE Trans. Appl. Supercond. **7**, 3840 (1997).

[15] P. Krkotić, Q. Gallardo, N. Tagdulang, M. Pont, and J. O'Callaghan, Algorithm for resonator parameter extraction from symmetrical and asymmetrical transmission responses, IEEE Trans. Microwave Theory Tech. **69**, 3917 (2021).

[16] D. Kajfez and P. Guillon, *Dielectric Resonators (Artech House Microwave Library)* (Noble Publishing Corporation, Atlanta, GA, 1998).

[17] J. Breeze, *Temperature and Frequency Dependence of Complex Permittivity in Metal Oxide Dielectrics: Theory, Modelling and Measurement*, Springer Theses (Springer International Publishing, New York, 2016).

[18] P. Krkotic, Evaluation of the surface impedance of ReBCO coated conductors and requirements for their use as beam screen materials for the FCC-hh, CERN Report No. CERN-THESIS-2022-281, 2023, https://cds.cern.ch/record/2846227.

[19] S. Calatroni, M. Arzeo, S. Aull, M. Himmerlich, P. Costa Pinto, W. Vollenberg, B. Di Girolamo, P. Cruikshank, P. Chiggiato, D. Bajek, S. Wackerow, and A. Abdolvand, Cryogenic surface resistance of copper: Investigation of the impact of surface treatments for secondary electron yield reduction, Phys. Rev. Accel. Beams **22**, 063101 (2019).

[20] P. Costa Pinto, S. Calatroni, H. Neupert, D. Letant-Delrieux, P. Edwards, P. Chiggiato, M. Taborelli, W. Vollenberg, C. Yin-Vallgren, J. Colaux, and S. Lucas, Carbon coatings with low secondary electron yield, Vacuum **98**, 29 (2013).